Identification of Genes Encoding Enzymes Catalyzing the Early Steps of Carrot Polyacetylene Biosynthesis[1][OPEN]

Lucas Busta,[a] Won Cheol Yim,[b] Evan William LaBrant,[a] Peng Wang,[c] Lindsey Grimes,[b] Kiah Malyszka,[b] John C. Cushman,[b] Patricia Santos,[b] Dylan K. Kosma,[b] and Edgar B. Cahoon[a,2,3]

[a]Center for Plant Science Innovation and Department of Biochemistry, University of Nebraska–Lincoln, Lincoln, Nebraska, 68588

[b]Department of Biochemistry and Molecular Biology, University of Nevada, Reno, Nevada 89557

[c]Tropical Crops Genetic Resources Institute, Chinese Academy of Tropical Agricultural Sciences, Danzhou, Hainan 571737, China

ORCID IDs: 0000-0002-0102-9986 (L.B.); 0000-0002-7489-0435 (W.C.Y.); 0000-0003-0742-9363 (E.W.L.); 0000-0002-1829-4321 (L.G.); 0000-0002-5561-1752 (J.C.C.); 0000-0002-3030-9207 (P.S.); 0000-0002-7277-1176 (E.B.C.)

Polyacetylenic lipids accumulate in various Apiaceae species after pathogen attack, suggesting that these compounds are naturally occurring pesticides and potentially valuable resources for crop improvement. These compounds also promote human health and slow tumor growth. Even though polyacetylenic lipids were discovered decades ago, the biosynthetic pathway underlying their production is largely unknown. To begin filling this gap and ultimately enable polyacetylene engineering, we studied polyacetylenes and their biosynthesis in the major Apiaceae crop carrot (*Daucus carota* subsp. *sativus*). Using gas chromatography and mass spectrometry, we identified three known polyacetylenes and assigned provisional structures to two novel polyacetylenes. We also quantified these compounds in carrot leaf, petiole, root xylem, root phloem, and root periderm extracts. Falcarindiol and falcarinol predominated and accumulated primarily in the root periderm. Since the multiple double and triple carbon-carbon bonds that distinguish polyacetylenes from ubiquitous fatty acids are often introduced by Δ12 oleic acid desaturase (FAD2)-type enzymes, we mined the carrot genome for *FAD2* genes. We identified a *FAD2* family with an unprecedented 24 members and analyzed public, tissue-specific carrot RNA-Seq data to identify coexpressed members with root periderm-enhanced expression. Six candidate genes were heterologously expressed individually and in combination in yeast and Arabidopsis (*Arabidopsis thaliana*), resulting in the identification of one canonical FAD2 that converts oleic to linoleic acid, three divergent FAD2-like acetylenases that convert linoleic into crepenynic acid, and two bifunctional FAD2s with Δ12 and Δ14 desaturase activity that convert crepenynic into the further desaturated dehydrocrepenynic acid, a polyacetylene pathway intermediate. These genes can now be used as a basis for discovering other steps of falcarin-type polyacetylene biosynthesis, to modulate polyacetylene levels in plants, and to test the in planta function of these molecules.

Many organisms implement specialized biochemical pathways to convert ubiquitous metabolites into bioactive chemical compounds. Since plants comprise the majority of the human diet, specialized plant metabolites play crucial roles not only in crop biology but also in human nutrition. Some asterids produce lipid compounds called polyacetylenes (for review, see Negri, 2015) that exhibit antifungal activity (Garrod et al., 1978; Kemp, 1978; Harding and Heale, 1980, 1981; Olsson and Svensson, 1996) and accumulate in response to fungal phytopathogen attack (De Wit and Kodde, 1981; Elgersma and Liem, 1989). These observations have led to the longstanding hypothesis that polyacetylenes are natural pesticides. These same lipid compounds exhibit cytotoxic activity against human cancer cell lines and slow tumor growth (Fujimoto and Satoh, 1988; Matsunaga et al., 1989, 1990; Cunsolo et al., 1993; Bernart et al., 1996; Kobaek-Larsen et al., 2005; Zidorn et al., 2005), making them important nutritional compounds.

The major source of polyacetylenes in the human diet is carrot (*Daucus carota* L.). Carrot is one of the most important crop species in the Apiaceae, with rapidly increasing worldwide cultivation (Rubatzky et al., 1999; Dawid et al., 2015). The most common carrot polyacetylenes are C_{17} linear aliphatic compounds containing two conjugated carbon-carbon triple bonds, one or two carbon-carbon double bonds, and a diversity of additional in-chain oxygen-containing functional groups. In carrot, the most abundant of these compounds are

[1]This research was supported by a National Science Foundation grant (Plant Genome IOS-13-39385 to E.B.C.) and a National Science Foundation of China grant (no. 31300260 to P.W.).

[2]Author for contact: ecahoon2@unl.edu.

[3]Senior author.

The author responsible for distribution of materials integral to the findings presented in this article in accordance with the policy described in the Instructions for Authors (www.plantphysiol.org) is: Edgar B. Cahoon (ecahoon2@unl.edu).

L.B., W.C.Y., P.S., D.K.K., and E.B.C. designed the research plans; L.B., W.C.Y., E.W.L., L.G., K.M., P.S., and P.W. performed the experiments; L.B. and W.C.Y. analyzed the data and prepared figures; L.B. wrote the article with contributions from all other authors; J.C.C. provided research oversight to W.C.Y.; E.B.C. supervised the research.

[OPEN]Articles can be viewed without a subscription.

www.plantphysiol.org/cgi/doi/10.1104/pp.18.01195

falcarinol and falcarindiol (Dawid et al., 2015). Based on their structures, it has been hypothesized that these compounds (alias falcarin-type polyacetylenes) are derived from ubiquitous fatty acids. Indeed, biochemical investigations (Haigh et al., 1968; Bohlman, 1988), radio-chemical tracer studies (Barley et al., 1988), and the discovery of pathway intermediates (Jones et al., 1966; Kawazu et al., 1973) implicate a diversion of flux away from linolenate biosynthesis as the entry point into falcarin-type polyacetylene biosynthesis (for review, see Minto and Blacklock, 2008).

The final steps of linolenate biosynthesis are the conversion of oleate to linoleate, mediated by fatty acid desaturase 2 (FAD2), and linoleate to linolenate, catalyzed by FAD3. Some plant species contain divergent forms of FAD2 that, instead of or in addition to converting oleate to linoleate, catalyze the installation of unusual in-chain functional groups such as hydroxyl groups, epoxy groups, conjugated double bonds, or carbon-carbon triple bonds into the acyl chain (Badami and Patil, 1980) and thus divert flux from linolenate production into the accumulation of unusual fatty acids. Previous work in parsley (*Petroselinum crispum*; Apiaceae) identified a divergent form of FAD2 that (1) was up-regulated in response to pathogen treatment and (2) when expressed in soybean embryos resulted in production of the monoyne crepenynate and, by the action of an unassigned enzyme, dehydrocrepenynate (Kirsch et al., 1997; Cahoon et al., 2003).

The results of the parsley studies are consistent with a pathogen-responsive, divergent FAD2-mediated pathway that leads to acetylenic fatty acids. However, information regarding the branch point into acetylenic fatty acid production in agriculturally relevant carrot is still largely missing, in particular, the identification and functional characterization of enzymes that can divert carbon flux away from linolenate biosynthesis into the production of dehydrocrepenynate and ultimately falcarin-type polyacetylenes. Such genes, once identified, could be used in the future design of transgenic carrot lines with altered polyacetylene content, enabling direct testing of in planta polyacetylene function and potentially the engineering of pathogen-resistant, more nutritious carrots. These genes could also provide the foundation for further investigations of more basic aspects of plant biology, including the evolution of fatty acid-derived natural product biosynthesis pathways across the Asterid clade, as well as the role of these pathways and compounds in plant ecology and plant defense.

Recently, a high-quality carrot genome assembly was released (Iorizzo et al., 2016), providing a foundation for genome-enabled studies of Apiaceous species. This study also provided publicly accessible RNA sequencing (RNA-Seq) data from diverse carrot tissues. Using these resources, this study aimed to provide a detailed gas chromatography-based quantification of polyacetylenes in carrot tissues for which RNA-Seq data are available, then combine this information with bioinformatics analysis and heterologous expression to identify and characterize biosynthetic genes that underlie the major entry point into carrot polyacetylene biosynthesis. To achieve these goals, thin-layer chromatography (TLC) was combined with gas chromatography-mass spectrometry (GC-MS) and gas chromatography-flame ionization detection to identify and quantify polyacetylenic metabolites in five different carrot tissues. Then the sequences and tissue expression profiles of potential *FAD2* and *FAD2*-like genes annotated in the *D. carota* genome were compared with the metabolite data to identify candidate pathway genes, followed by biochemical functionality tests using yeast (*Saccharomyces cerevisae*) and Arabidopsis (*Arabidopsis thaliana*) as heterologous expression systems.

RESULTS

Identification and Quantification of Carrot Polyacetylenes Using GC-MS

To identify carrot polyacetylenes, TLC was used to fractionate ethyl acetate extracts from carrot taproots. Compounds in the fractions recovered from TLC plates were converted into their trimethylsilyl (TMS) derivatives and analyzed with GC-MS. Several fractions contained only monoacylglycerols, triterpenoids, or coumarins, and were not studied further, leaving four fractions potentially containing polyacetylenes. In order of their migration on the TLC plate, the first three each contained a single compound (compounds **1.1**, **2.1**, and **3.1**; Fig. 1, A–C), while the fourth contained two compounds (**4.1** and **4.2**, Fig. 1D). Compounds **1.1** and **3.1** generated mass spectra that matched those of synthetic standards for the well-described carrot polyacetylenes falcarinol and falcarindiol, respectively (Supplemental Fig. S1; Kosma et al., 2015) and were identified as such, leaving the structures of compounds **2.1**, **4.1**, and **4.2** to be determined.

To increase the relative abundance of high-mass fragments and gain additional structural information, the four fractions were reanalyzed using 40 eV, 20 eV, and 10 eV ionization energies in addition to the conventional 70 eV, then all the spectra acquired for each **1.1**, **2.1**, **3.1**, **4.1**, and **4.2** were merged to generate a composite spectrum for each compound. These spectra were used to conduct a detailed analysis of the electron impact fragmentation of TMS-derivatized polyacetylenes so that future research may incorporate electron impact mass spectrometry information into polyacetylene structure elucidations. The composite spectrum for falcarinol (**1.1**) contained peaks arising from its single TMS-derivatized hydroxyl group (mass-to-charge ratio (*m/z*) 73: $[Si(CH_3)_3]^+$, Fig. 1E), its polyunsaturated system (*m/z* 91: a tropylium ion), allylic cleavage near the midchain double bond (*m/z* 231 and 245; Fig. 1, E and J), and peaks indicating molecular weight (*m/z* 316:$[M]^+$, 301: $[M\text{-}CH_3]^+$). The mass spectrum of falcarindiol (**2.1**) contained peaks arising from two

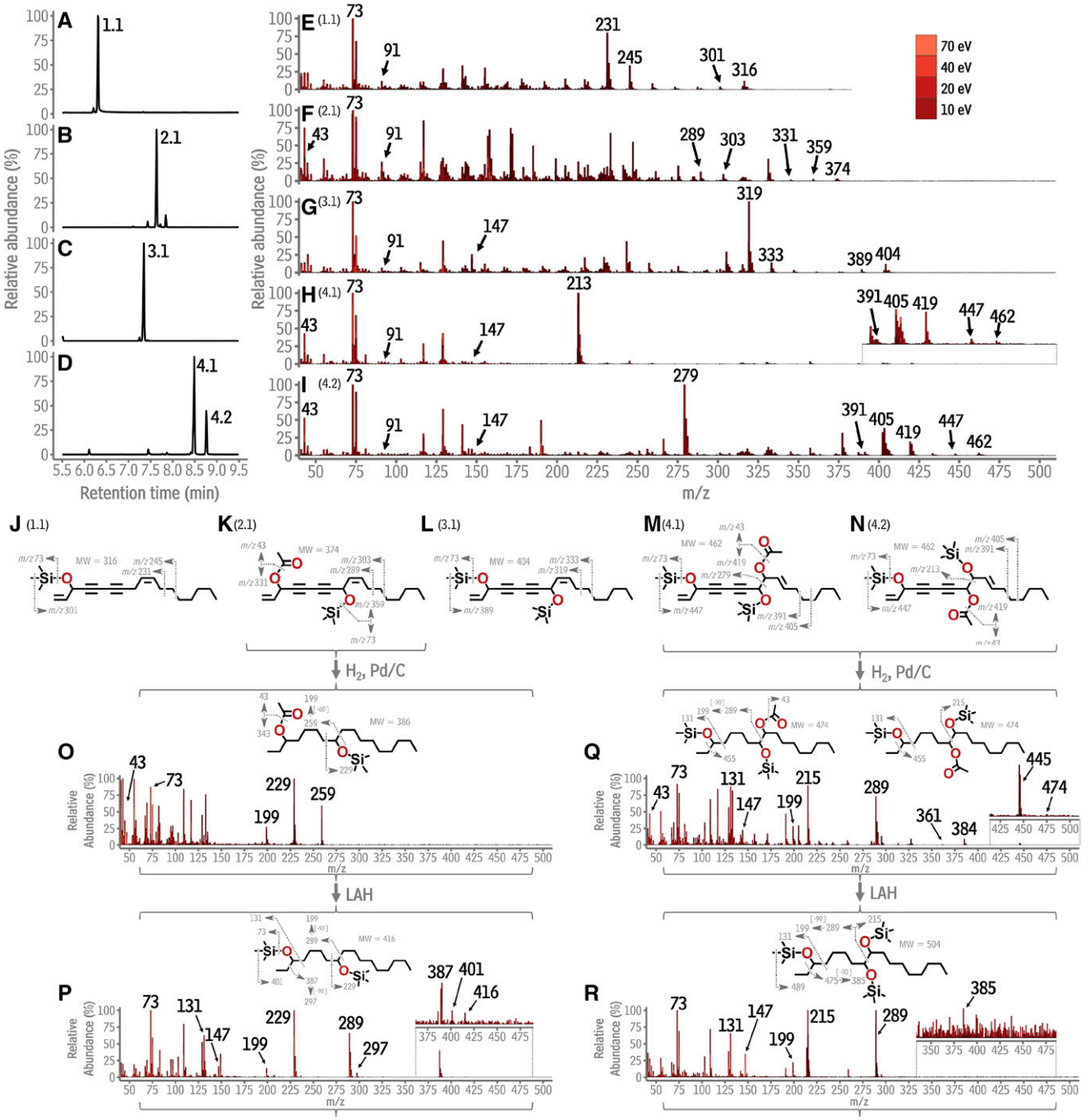

Figure 1. Gas chromatographic-mass spectrometric identification of polyacetylenes from *Daucus carota*. A to D, Total ion chromatograms of putative polyacetylene-containing TLC fractions. Each peak is labeled with a number (**1.1**, **2.1**, **3.1**, **4.1**, **4.2**) that refers to its underlying compound. E to I, Composite mass spectra for each numbered compound (**1.1**–**4.2**), generated by overlaying the spectrum acquired for each compound at 70, 40, 20, and 10 eV. J to N, Structures of the numbered compounds and likely fragmentation mechanisms giving rise to their spectra in E to I. O to R, Spectrum, structure, and fragmentation of the product obtained from hydrogenation of compounds **2.1**, **4.1** and **4.2**, respectively. *m*/z, mass to charge ratio; Pd/C, palladium on carbon; LAH, lithium aluminum hydride; eV, electron volts.

TMS-derivatized hydroxyl groups (*m*/z 73, *m*/z 147: $[(CH_3)_3SiOSi(CH_3)_3]^+$), its polyunsaturated system (*m*/z 91) and allylic cleavage (*m*/z 391 and 333, Fig. 1L), and molecular weight indicators (*m*/z 404: $[M]^+$, *m*/z 389: $[M\text{-}CH_3]^+$). Unlike saturated aliphatics with secondary hydroxyl groups, these polyacetylenes did not

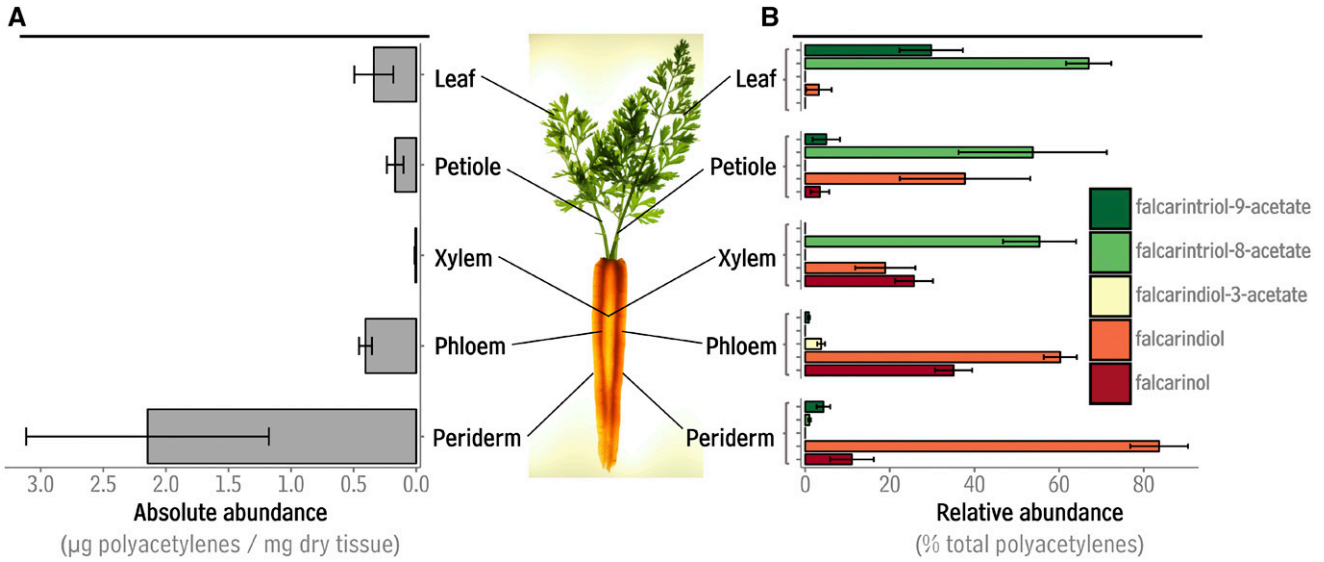

Figure 2. Polyacetylene abundance and composition in aerial and subterranean tissues of *Daucus carota*. A, Absolute abundance of polyacetylenes in leaf, petiole, xylem, phloem, and epidermis given in micrograms per milligram of dry tissue. B, Relative abundance of polyacetylenes in leaf, petiole, xylem, phloem, and epidermis given as percent of total polyacetylenes. For both A and B, bar lengths and error bars represent the average and SD of six independent samples each from a different carrot plant.

generate strong α-fragments, likely because the secondary hydroxyl groups are flanked by double or triple C-C bonds on all sides.

TLC and GC retention behavior indicated that **2.1** had a polarity intermediate to and a boiling point higher than falcarinol and falcarindiol (Fig. 1, A–C). Its composite spectrum contained peaks indicating that TMS-derivatized **2.1** had one acetylated hydroxyl group (*m/z* 43: $[COCH_3]^+$, Fig. 1F), one TMS-derivatized hydroxyl group (*m/z* 73), a polyunsaturated system (*m/z* 91), as well as a molecular weight of 374 (*m/z* 374: $[M]^+$, *m/z* 359: $[M\text{-}CH_3]^+$, and *m/z* 331: $[M\text{-}COCH_3]^+$), thus suggesting a C_{17} compound with two hydroxyl groups (one acetylated) flanked on all sides by double or triple bonds with six degrees of unsaturation. These mass spectral features led to the hypothesis that **2.1** was falcarindiol-3-acetate (Fig. 1K), a previously described carrot polyacetylene, which was then tested by hydrogenating **2.1**. The spectrum of the TMS-derivatized hydrogenation product had peaks corresponding to one acetylated hydroxyl group (*m/z* 43: $[COCH_3]^+$, Fig. 2O), and one TMS-derivatized hydroxyl group on C-8 (*m/z* 73: $[Si(CH_3)_3]^+$, *m/z* 229 and 259: α-fragments, *and m/z* 199: *m/z* 259 α-fragment less $HOCOCH_3$). To verify the presence and position of the acetylated hydroxyl group, hydrogenated **2.1** was reduced. The composite spectrum of the TMS-derivatized reduction product had peaks indicating two TMS-derivatized hydroxyl groups (*m/z* 73 and 147, Fig. 1P) on C-3 and C-8 (*m/z* 131, 387, 229, and 289:α-fragments; *m/z* 199 and 297: α-fragments minus $HOSi(CH_3)_3$), and a molecular weight of 416 (*m/z* 416: $[M]^+$, *m/z* 401: $[M\text{-}CH_3]^+$). Collectively, these features confirmed the following hydrogenation products: reduced **2.1** as heptadecane-3,8-diol (Fig. 1P), hydrogenated **2.1** as 8-hydroxyheptadecan-3-yl acetate (Fig. 1O), and **2.1** as falcarindiol-3-acetate (Fig. 2K).

TLC and GC behavior indicated that, relative to **1.1**, **2.1**, and **3.1**, compounds **4.1** and **4.2** had higher polarities and boiling points (Fig. 1, A–D). The composite spectra of TMS-derivatized **4.1** and **4.2** contained peaks indicating one acetylated hydroxyl group (*m/z* 43; Fig. 1, H and I), two TMS-derivatized hydroxyl groups (*m/z* 73 and *m/z* 147), a polyunsaturated system (*m/z* 91), and a molecular weight of 462 (*m/z* 462: $[M]^+$, *m/z* 419: $[M\text{-}COCH_3]^+$, and *m/z* 447: $[M\text{-}CH_3]^+$), suggesting **4.1** and **4.2** as isomeric C_{17} compounds with three hydroxyl groups (one acetylated) and six degrees of unsaturation. **4.1** and **4.2** also generated prominent mass spectral peaks at *m/z* 213 and *m/z* 279, respectively. These were highly reminiscent of secondary hydroxyl group α-fragments and suggested that double or triple bonds flanked each oxygen-containing secondary functional group in **4.1** and **4.2**, except one side of one group around which a single α-fragment could be generated. Considering this evidence and the trifunctional falcarindiolone acetates previously identified in carrot (Schmiech et al., 2009), we hypothesized that **4.1** and **4.2** were the falcarintriol acetates 3,8-dihydroxyheptadeca-1,10-dien-4,6-diyn-9-yl acetate and 3,9-dihydroxyheptadeca-1,10-dien-4,6-diyn-8-yl acetate, respectively (aliases falcarintriol-9-acetate and falcarintriol-8-acetate; Fig. 1, M and N).

To test the structural hypotheses for **4.1** and **4.2**, a mixture of the two was hydrogenated. GC-MS analysis of the reaction product yielded a single chromatographic

peak, suggesting that it might be composed of two coeluting compounds. The composite mass spectrum from this chromatographic peak indicated that the compound(s) had one acetylated hydroxyl group (*m/z* 43), two TMS-derivatized hydroxyl groups (*m/z* 73 and 147), one of which was on C-3 (*m/z* 131 and 455: α-fragments), and a molecular weight of 474 (*m/z* 474: $[M]^+$). It also suggested TMS-derivatized secondary hydroxyl groups on C-8 and C-9 (*m/z* 215 and 289: α-fragments, *m/z* 199: $HOSi(CH_3)_3$ loss from *m/z* 289, Fig. 1Q). Thus, the structural evidence pointed to the product of the hydrogenation reaction being comprised of a mixture of 3,9-dihydroxyheptadecan-8-yl acetate and 3,8-dihydroxyheptadecan-9-yl acetate. To verify this assignment, the hydrogenation reaction products were reduced. The composite spectrum from the single resulting GC peak suggested an underlying compound with three TMS-derivatized hydroxyl groups on C-3, C-8, and C-9 (*m/z* 73 and 147; *m/z* 131, 215, and 289: α-fragments; and *m/z* 199 and 385: $HOSi(CH_3)_3$ loss from the α-fragments). Overall, this spectrum was consistent with heptadecane-3,8,9-triol, providing further support for the structures of **4.1** and **4.2** as 3,8-dihydroxyheptadeca-1,10-dien-4,6-diyn-9-yl acetate and 3,9-dihydroxyheptadeca-1,10-dien-4,6-diyn-8-yl acetate (aliases, falcarintriol-8-acetate and falcarintriol-9-acetate).

Having analyzed the structures of the carrot polyacetylenes that were detected using GC-MS, the next objective was to measure their tissue-specific accumulation. Total polyacetylene content was highest in taproot peridermal tissues at 2.1 µg/mg dry tissue, while phloem, xylem, petiole, and leaf tissues contained approximately 0.41, 0.01, 0.16, 0.34 µg/mg dry tissue, respectively (Fig. 2A). In taproot periderm, falcarindiol was the primary polyacetylene (comprising 83% of the total; Fig. 2B). In phloem, both falcarindiol and falcarinol were present in substantial amounts (60% and 35%). Xylem tissue contained mainly falcarintriol-8-acetate (53%), together with falcarinol and falcarindiol (25% and 18%). Petioles bore mainly falcarintriol-8-acetate (57%) together with falcarinol (37%), while leaves contained falcarintriol-8-acetate (67%) and falcarintriol-9-acetate (30%).

Identification and Functional Testing of Candidate Carrot Polyacetylene Biosynthesis Genes

With the structural and quantitative analyses of carrot polyacetylenes complete, the next objective was to identify and functionally characterize genes catalyzing early steps in their biosynthetic pathway. Based on previous work in *P. crispum* (Cahoon et al., 2003), *FAD2* genes were targeted. Searching the carrot genome revealed a very large number of *FAD2* genes, 24 in total, distributed across chromosomes 1 and 3 to 8 (Supplemental Fig. S2). The amino acid sequences of the predicted proteins encoded by these genes were aligned with previously characterized FAD2 sequences (Supplemental Fig. S3). Each of the 24 carrot FAD2s contained His boxes typical of FAD2-type redox enzymes (Fig. 3, yellow highlights) consistent with the central role of these residues in coordinating metal atoms required for redox activity (Shanklin et al., 1994). Next, the amino acids occupying each position in known canonical FAD2s versus known divergent FAD2s (i.e. FAD2s that catalyze reactions other than Δ12 oleate desaturation, such as hydroxylation, double bond conjugation, and acetylenation) were examined, revealing certain positions in which amino acid identity segregated between the two groups of FAD2s (Fig. 3, pink highlights). In these positions, just like many previously reported FAD2-like proteins with divergent function, 20 of the carrot FAD2s contained conspicuous amino acid substitutions, some of which were near conserved His boxes. Using the nucleotides underlying a subset of the amino acid alignment that included both the positions surrounding the conserved His-rich motifs as well as positions with amino acids that segregated between canonical FAD2s and functionally divergent FAD2s, a maximum likelihood tree was created to visualize how the carrot nucleotide sequence subsetsgrouped with previously identified *FAD2s*. This tree contained two major clades, one composed primarily of previously characterized *FAD2* desaturases as well as four carrot *FAD2s* (clade of mostly blue tips, Fig. 3), while the other clade was composed largely of known divergent *FAD2s* and 20 carrot *FAD2*-like sequences (clade of mostly green tips, Fig. 3).

Having identified which carrot FAD2s were likely canonical and likely divergent, a transcriptomics approach was used to better prioritize polyacetylene biosynthesis-related FAD2s and FAD2-likes for functional testing. First, public RNA-Seq data from 20 diverse carrot tissues were aligned to the carrot genome (Iorizzo et al., 2016). These alignments were used to quantify transcriptome expression levels with raw read counts and were then normalized to transcripts per kilobase million (TPM) to determine transcript abundances. Sinceit was observed in parallel that average polyacetylene abundance in taproot tissues increased in response to pathogen treatment (Supplemental Fig. S4), and previous work had demonstrated that functional *FAD2* desaturase and acetylenase genes from other Apiales species are up-regulated in response to fungal elicitors both in planta and in cell suspensions (Kirsch et al., 1997; Cahoon et al., 2003), RNA-Seq was performed both before and 8 h after treatment with a fungal elicitor to obtain additional information about the 24 carrot *FAD2* genes. To ensure that the carrots were not elicited by ambient fungi prior to the experimental treatment, suspensions of carrot callus cells were used in place of greenhouse-grown carrots. Using both the public RNA-Seq data and the RNA-Seq data from the cell elicitation, the expression profiles of the 24 carrot *FAD2*-like genes were compared. The expression of a gene encoding a putative canonical FAD2 Δ12 desaturase (DCAR_013547) was up-regulated both in whole root tissue and, on average, in response to fungal elicitation (Fig. 4A; Supplemental Figs. S5 and S6A). Based

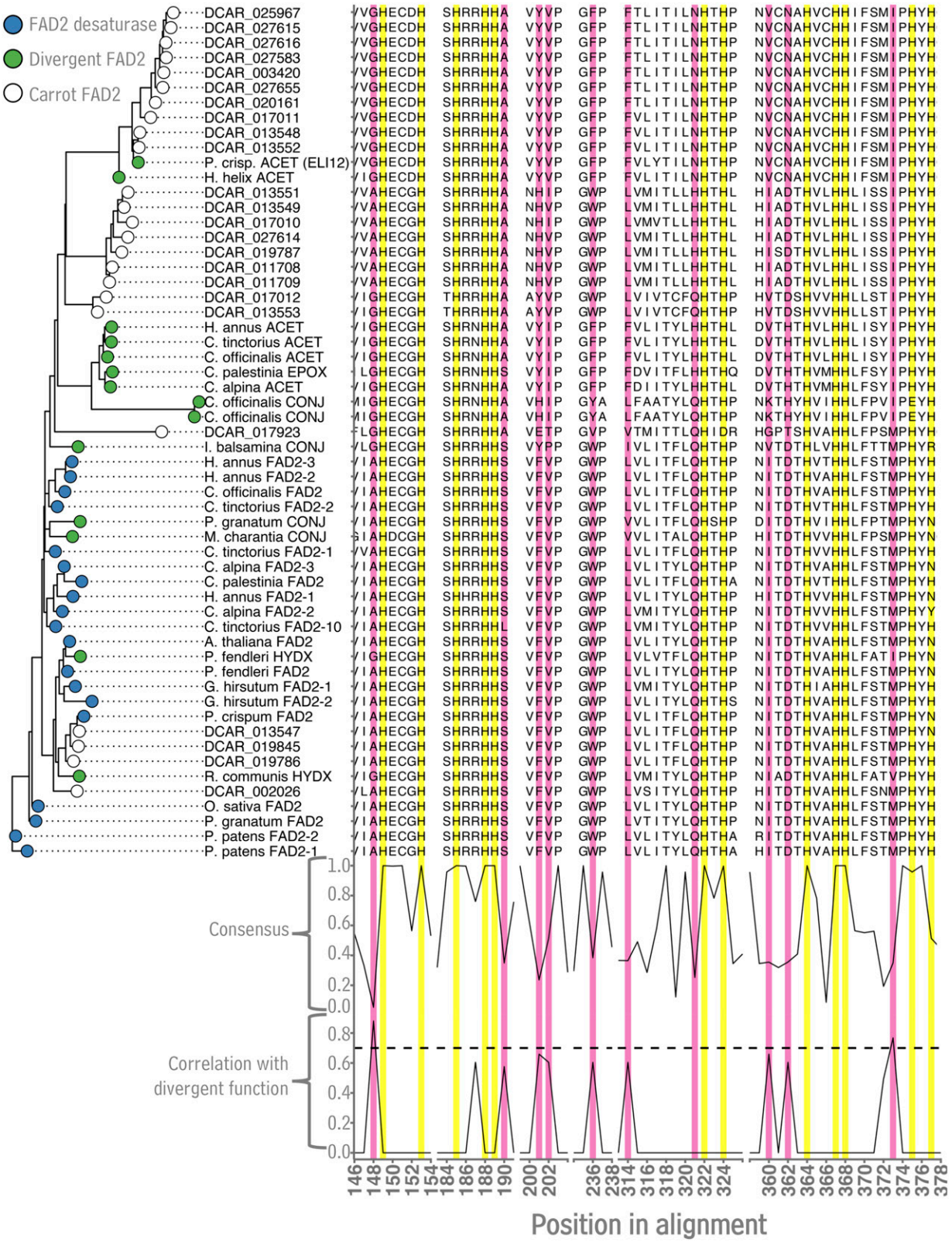

Figure 3. Analysis of FAD2 amino acid sequences from carrot *Daucus carota*. Subsets of the multiple sequence alignment of carrot FAD2 sequences and previously characterized FAD2 enzymes from other plant species. Subsets were chosen based on the presence of highly conserved His residues (yellow highlights, "consensus" score on bottom) and residues associated with Δ12 desaturase versus divergent FAD2 activity (pink highlights, "correlation with divergent function" score on bottom).

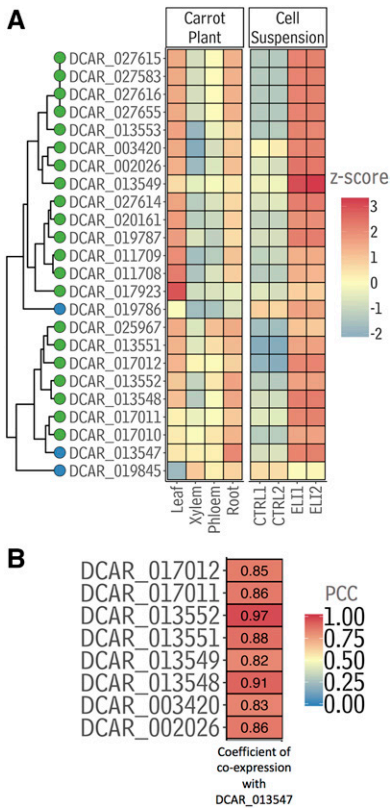

Figure 4. Expression of *FAD2s* from carrot. A, Expression of carrot *FAD2* genes (plotted as z-scores) in carrot leaves, xylem, phloem, and whole-root samples, as well as in carrot suspension cultures before (CTRL1 and 2, i.e. two replicates) and after (ELI1 and 2, i.e. two replicates) treatment with an elicitor extracted from mycelia of *Phytopthora megasperma*. The dendrogram connecting the gene names on the *y* axis was generated from ward. D2 clustering analysis of the z-scores presented in Supplemental Figure S5, not the heat map presented in A, which shows a subset of the full heat map presented in Supplemental Figure S5. Blue tip points denote putative *Δ12 FAD2 desaturase* genes and green tips denote putative divergent *FAD2s* as determined by the clustering in Fig. 3. B, Coexpression between *DCAR_013547* and other carrot *FAD2s* with a Pearson correlation coefficients $q < 0.1$. Sequence data used in this figure can be found in the Phytozome/GenBank databases under the accession numbers listed in Supplemental Table S3.

on this information, this gene became the best candidate for encoding a Δ12 desaturase associated with the carrot polyacetylene pathway.

To test for desaturase activity, *DCAR_013547* (desaturase 1; Fig. 5A) was expressed in yeast cultures using an inducible promoter. GC analysis of transmethylated yeast revealed that induced cultures expressing the empty vector contained mainly oleate (Fig. 5, B and C). The GC trace from the cultures expressing *DCAR_013547* contained an additional peak (Fig. 5D) that had a retention time and mass spectrum identical to that of linoleate (Fig. 5, B versus D, and Fig 5., E versus F), indicating that DCAR_013547 has Δ12 desaturase activity. Using the same approach, the catalytic ability of two other putative carrot FAD2 Δ12 desaturases, DCAR_019786 and DCAR_019845, were tested (Supplemental Fig. S7), indicating that these are also able to catalyze Δ12 desaturation.

Having identified a canonical *FAD2* with periderm-enhanced expression, the next objective was to identify a Δ12 acetylenase from carrot (acetylenase 1; Fig. 5A). For this, a coexpression matrix for carrot *FAD2(*-like*)s* was developed. After filtering for genes with Pearson correlation coefficient (PCC) p values < 0.1, the *FAD2*-like gene most strongly coexpressed with the bait was *DCAR_013552* (PCC = 0.97; Fig. 4). Collective consideration of phylogenetic relationships (Fig. 3), expression profiles as determined by RNA-Seq (Fig. 4A) and confirmed by reverse transcription quantitative PCR (RT-qPCR; Supplemental Fig. S6), and the coexpression network analysis (Fig. 4B), led to the identification of DCAR_017011 and DCAR_01354 as secondary candidates for Δ12 acetylenases. To functionally characterize the genes encoding these proteins, each was expressed under the control of a seed-specific promoter in the Arabidopsis double mutant *fad3fae1*, which accumulates a large amount of linoleate in its seeds. To test for specific FAD2 activities, transgenic Arabidopsis seeds were analyzed at the T1 stage, similar to a previously reported FAD2 screen (Cahoon and Shanklin, 2000) and analogous to studies in which enzyme activity is assessed using infiltration-mediated expression in *Nicotiana benthamiana*. Relative to the empty vector control, the GC traces of transmethylated T1 seed fatty acids from seeds expressing each of the putative acetylenases contained an additional peak with retention time and mass spectrum identical to the crepenynate standard (Fig. 5; Supplemental Fig. S7), confirming that DCAR_013552, DCAR_017011, and DCAR_013548 are enzymes with Δ12 acetylenase activity. To determine if these divergent FAD2 enzymes exhibit Δ12 desaturation function in addition to their divergent function, as has been observed for other plant FAD2s (Sperling et al., 2000), the gene encoding each was cloned into pYES yeast expresion vectors and transformed into yeast. Analysis of fatty acids in induced yeast cultures containing empty vectors versus vectors harboring *DCAR_013552*, *DCAR_017011*, and *DCAR_013548* revealed no additional peaks, indicating that proteins encoded by these genes do not catalyze desaturation of oleate in the Δ12 position in addition to acetylenation of linoleate in the Δ12 position.

Figure 3. (*Continued*.)
The maximum likelihood phylogenetic tree was generated using nucleotide sequences underlying the amino acids shown in alignment subsets. Sequence data used in this figure can be found in the Phytozome/GenBank databases under the accession numbers listed in Supplemental Table S3.

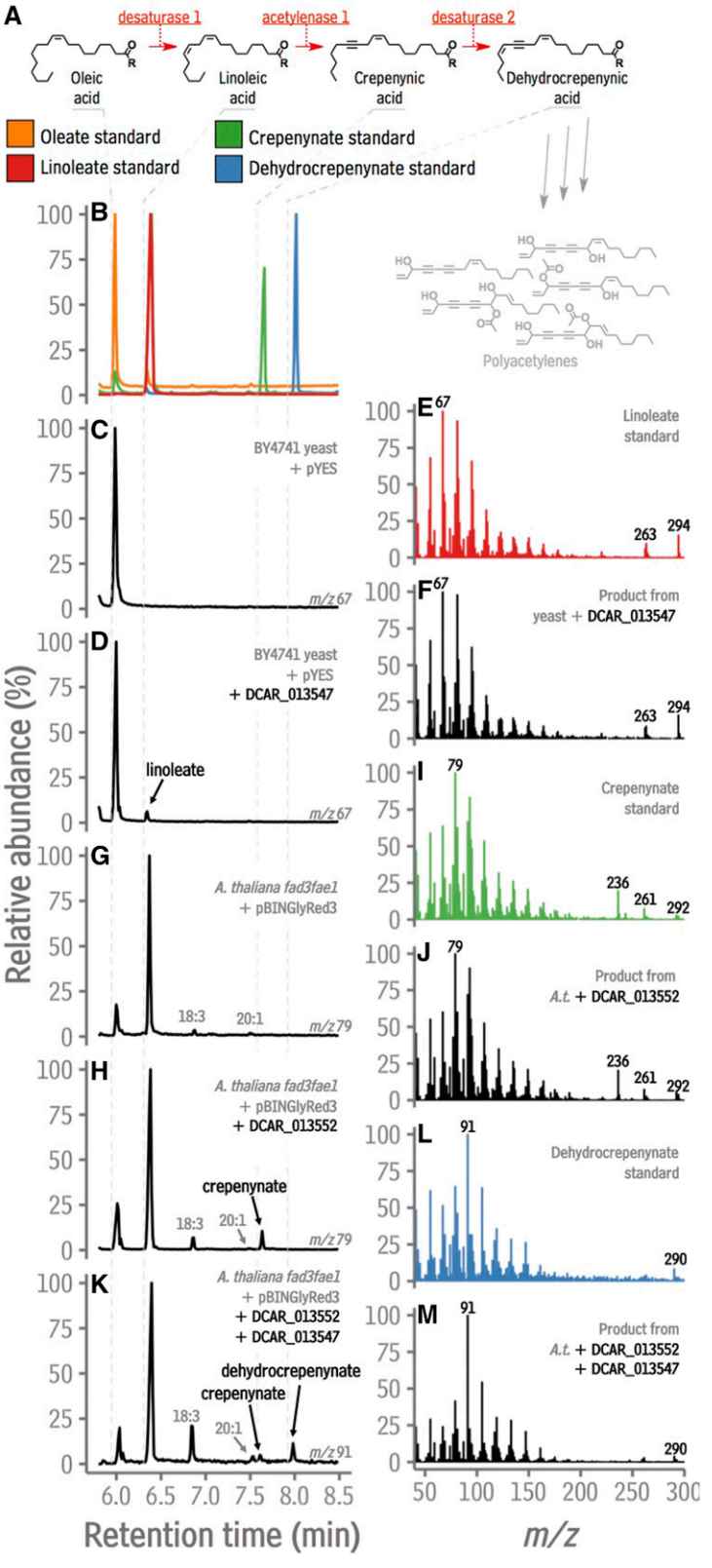

Figure 5. Functional testing of candidate carrot desaturase and acetylenase enzymes by heterologous expression. A, Pathway to falcarin-type polyacetylenes. B, GC traces (ion abundance versus time) of oleate, linoleate, crepenynate, and dehydrocrepenynate standards. C, Single ion trace (*m/z* 67) of the fatty acid methyl esters from induced yeast strain BY4741 containing the pYES vector. D, Single ion trace (*m/z* 67) of the fatty acid methyl esters from induced yeast strain BY4741 containing the pYES vector harboring DCAR_013547. E, EI mass spectrum of the linoleate standard. F, EI mass spectrum of the indicated peak in D. G, Single ion trance (*m/z* 79) of fatty acid methyl esters from Arabidopsis *fad3fae1* seeds transformed with an empty the pBINGlyRed3 vector. H, Single ion trance (*m/z* 79) of the fatty acid methyl esters from Arabidopsis *fad3fae1* seeds transformed with the pBINGlyRed3 vector harboring DCAR_013552. I, EI mass spectrum of the crepenynate standard. J, EI mass spectrum of the indicated peak in H. K, Single ion trance (*m/z* 91) of the fatty acid methyl esters from Arabidopsis *fad3fae1* seeds transformed with the pBINGlyRed3 vector harboring both DCAR_013547 and DCAR_013552. L, EI mass spectrum of the dehydrocrepenynate standard. M, EI mass spectrum of the indicated peak in K. *m/z*, mass to charge ratio. Sequence data used in this figure can be found in the Phytozome/GenBank databases under the accession numbers listed in Supplemental Table S3.

Last, a Δ14 desaturase capable of converting crepenynate into dehydrocrepenynate (desaturase 2; Fig. 5A) was sought. Previously, heterologous expression in yeast was used to determine that a fungal FAD2 has both Δ12 linoleate desaturase activity and Δ14 crepenynate desaturase activity (Blacklock et al., 2010). In the present work, this led to the hypothesis that DCAR_013547 (a Δ12 desaturase) might also catalyze Δ14 crepenynate

desaturation. To test this hypothesis, *DCAR_013547* was expressed both alone (in a high-linoleate background) and together with *DCAR_013552* (i.e. in a background containing crepenynate). GC analysis of transgenic, high-linoleate seeds (*Arabidopsis fad3fae1*) expressing *DCAR_013547* under control of a seed-specific promoter did not reveal any additional peaks compared to the empty vector control (Supplemental Fig. S7). However, GC analysis of transgenic *Arabidopsis fad3fae1* seeds harboring both *DCAR_013552* (the Δ12 acetylenase) and *DCAR_013547* revealed not only the production of crepenynate (the product of the Δ12 acetylenase DCAR_013552), but also the accumulation of dehydrocrepenynate (Fig. 5, H versus K, and Fig. 5, L versus M). This observation, together with the result from the expression of *DCAR_013547* in yeast (Fig. 5, B versus D, and Fig. 5, E versus F), strongly implicates DCAR_013547 as a bifunctional enzyme capable of catalyzing both Δ12 desaturation of oleate and Δ14 desaturation of crepenynate. Since another carrot Δ12 oleate desaturase (DCAR_019786) was also upregulated during elicitation, we used the same approach described above to determine if it also had Δ14 crepenynate desaturase activity. Arabidopsis *fad3fae1* seeds harboring DCAR_013552 alone accumulated crepenynate (Fig. 5), but seeds transformed with a vector harboring both *DCAR_013552* and *DCAR_019786* produced both crepenynate and dehydrocrepenynate (Supplemental Fig. S8), indicating that DCAR_019786 can also catalyze Δ14 crepenynate desaturation in addition to Δ12 oleate desaturation.

DISCUSSION

The objectives of this study were first to identify and quantify polyacetylenes in diverse carrot tissues, then to correlate this information with RNA-Seq data to identify putative polyacetylene biosynthesis genes, and finally to functionally characterize candidate genes using heterologous expression systems. These pursuits led to several major findings, which include (1) the tentative identification of two novel polyacetylenes, falcarintriol-8-acetate and falcarintriol-9-acetate, by GC-MS, (2) that polyacetylenes accumulate primarily in the periderm of carrot taproots, (3) that the carrot genome contains 24 *FAD2*(-like) sequences, several of which exhibit enhanced expression in the taproot periderm, (4) that at least three of these genes encode Δ12 oleate desaturases, at least three encode Δ12 linoleate acetylenases, and (5) that at least two of the Δ12 oleate desaturases catalyze Δ14 crepenynate desaturation. These new findings can now be integrated to discuss the specificity and structural features of FAD2 desaturases and acetylenases, as well as the biosynthesis and structural diversity of falcarin-type polyacetylenes.

Specificity and Structural Features of Carrot FAD2 Desaturases and Acetylenases

This study identified an unprecedented number (24) of *FAD2* sequences in a plant (Supplemental Fig. S2). The identification of a high number of *FAD2* sequences (18) in parsley (Somssich et al., 1989) suggests that other Apiaceae may also contain a high number of these genes. The six carrot *FAD2* and *FAD2*-like sequences functionally characterized here reside close to one another on carrot chromosome four (Supplemental Fig. S2). Based on microsyntenic and phylogenomic analyses (Supplemental Fig. S9), this region appears to have experienced local tandem duplications. In this work, a heterologous expression approach determined that, of the 24 carrot FAD2s, at least three are Δ12 oleate desaturases, at least three are Δ12 linoleate acetylenases, and at least two of the Δ12 desaturases are also Δ14 crepenynate desaturases that can produce dehydrocrepenynic acid (Fig. 5; Supplemental Figs. S7 and S8). Two previous reports also suggest that some Δ12 desaturases can, with a crepenynate substrate, produce dehydrocrepenynate via Δ14 desturation. In one, the expression of a *P. crispum* Δ12 acetylenase in soybean embryos resulted in the accumulation of both crepenynate and dehydrocrepenynate (Cahoon et al., 2003), suggesting that the endogenous soybean FAD2 Δ12 oleate desaturase was catalyzing Δ14 desaturation. In a second study, expressing a FAD2 from the fungus *Cantharellus formosus* in a high-oleate environment resulted in linoleate accumulation, while expressing the same enzyme in a crepenynate-containing background led to dehydrocrepenynate accumulation (Blacklock et al., 2010), thus demonstrating both Δ12 oleate desaturase and Δ14 crepenynate desaturase activity for that enzyme. These observations of bifunctionality in FAD2 Δ12 oleate desaturases from plant and fungal species raise the question of whether all FAD2 Δ12 oleate desaturases can catalyze Δ14 crepenynate desaturation. Here, crepenynate accumulated in Arabidopsis seeds without concomitant accumulation of dehydrocrepenynate, even in the presence of the endogenous Arabidopsis FAD2 Δ12 oleate desaturase. Similarly, the normal seed oil composition of, for example, *Crepis alpina*, accumulates substantial amounts of crepenynate (the biosynthesis of which is mediated in part by a canonical FAD2; Nam and Kappock, 2007), but no dehydrocrepenynate accumulates (Adlof and Emken, 1993). Thus, though some Δ12 oleate desaturases are clearly able to catalyze Δ14 crepenynate desaturation, this bifunctionality is almost certainly not a property of all Δ12 oleate desaturases.

Bifunctional FAD2 Δ12 and Δ14 desaturases are not the only enzymes that can catalyze fatty acid desaturation in two positions, as an enzyme from the soldier beetle *Chauliognathus lugubris* catalyzes both Δ14 crepenynate desaturation and Δ16 desaturation of 9Z-octadecen-12,14-diynoic acid (Haritos et al., 2012). This insect desaturase is another example of an enzyme that can catalyze desaturation in one position and then, after that same position has been acetylenated, can catalyze another desaturation two carbons further down the chain from the initial reaction site. It remains to be seen whether the structural modifications that enable Δ12/Δ14 desaturase bifunctionality in plants and fungi are

similar to those that enable Δ14/Δ16 desaturase bifunctionality in soldier beetles and whether this bifunctionality comes at the cost of lower Δ12 desaturation efficiency.

Aligning the amino acid sequences of the carrot FAD2s with those from other plants, it was apparent that the carrot FAD2s contained the His boxes typical of FAD2 enzymes, and 20 of the 24 carrot FAD2s contained conspicuous substitutions in positions near the active site histidines. A comparison of both canonical and divergent FAD2s from carrot and other species shows that some of these near-active-site substitutions are relatively well-conserved in divergent FAD2s, most notably the Ala-to-Gly substitution preceding the first His box and the Met-to-Ile substitution following the third His box (Fig. 3). Considering a structural model of a plant FAD2 desaturase (*P. crispum* FAD2; Supplemental Fig. S10) derived from the crystal structure of the *Homo sapiens* stearoyl-CoA desaturase (Wang et al., 2015), it seems possible that these two substitutions, especially the Ala-to-Gly, are quite close to each enzyme's reaction center and may well alter the geometries that can be occupied by the active site histidines and coordinated metal atoms. Such alterations may, in turn, modify the electronic environment of the active site and the outcome of the enzymatic reaction.

Previous studies of divergent FAD2 hydroxylases from *Physaria fendleri* and *Ricinus communis* that mainly catalyze oleate hydroxylation found that both the Gly-to-Ala as well as the Met-to-Ile substitutions mentioned above are major contributors to partitioning between canonical and diverged function of these enzymes (Broun et al., 1998; Broadwater et al., 2002). For carrot FAD2-like acetylenases, a similar pattern is observed (Fig. 3), suggesting that these residues may also play a role in partitioning between desaturase and acetylenase activities, as described previously (Cahoon and Kinney, 2005). However, it is worth noting that these substitutions are lacking in some divergent FAD2-like conjugases, including those from *Momordica charantia* and *Impatiens balsamina* (Cahoon et al., 1999), as well as *Punica granatum* (Hornung et al., 2002). Point mutation studies of FAD2-like hydroxylases suggest that other mutations may promote divergent FAD2 activity in the absence of the A/G and M/I substitutions. Still, these conjugases, along with observations of divergent FAD2 multifunctionality (for example, Δ12 oleate desaturation versus Δ12 palmitate desaturation versus Δ12 oleate hydroxylation by the *L. fendleri* FAD2; Broun et al., 1998; Broadwater et al., 2002), indicate that subtle changes in primary structure can exert considerable influence over the outcome of a FAD2-catalyzed reaction. This sensitivity is reminiscent of cytochrome P450 oxidoreductases, which also exhibit substantial catalytic plasticity in response to minor changes in primary structure (for review, see Pochapsky et al., 2010). Such plasticity is a signature of enzymes involved in specialized metabolic processes, such as the pathway to carrot polyacetylenes.

Polyacetylene Biosynthesis

We carried out a detailed, quantitative analysis of the distribution of carrot polyacetylenes and found that they are primarily located in the taproot periderm. This result is in agreement with a previous study that found higher polyacetylene levels in intact versus peeled carrots (Czepa and Hofmann, 2003), roughly similar to a Raman spectroscopic analysis of polyacetylene distributions in carrot root discs (Roman et al., 2011) and consistent with studies of other Apiales and Asterales in which polyacetylenes were found primarily (though not always) in the roots (Elgahme and Wittstock,2018). Here, we also identified enzymes capable of converting a basic monounsaturated fatty acid, oleic acid, into the polyunsaturated, acetylenic dehydrocrepenynic acid via three enzymatic transformations (Fig. 5). Our analysis of public RNA-Seq data and RT-qPCR data strongly suggest that the expression of these enzymes is enhanced in the taproot periderm (Fig. 4; Supplemental Fig. S6), the location of polyacetylene accumulation. Though it cannot be ruled out that polyacetylenes are synthesized in nonperidermal tissues and transported to the periderm, the data presented here implicate the periderm as the primary site of biosynthesis. The tissue specificity of both polyacetylene gene expression and metabolite accumulation is consistent with the long-suspected in planta function of these compounds: plant-microbe and/or plant-pathogen interactions. The genes identified here will be important tools for manipulating polyacetylene accumulation in carrot, enabling comparisons of pathogen resistance in polyacetylene-rich and polyacetlyene-lacking genotypes for the first time. These data also suggest that a periderm-specific transcriptomic analysis will be an important tool for elucidating the remaining steps in the pathway to falcarindiol.

Transcript tissue specificity is a characteristic that can be leveraged for gene discovery using coexpression network analysis (Wisecaver et al., 2017). In this work, identification of a single gene on a specialized metabolic pathway was followed with a coexpression analysis of tissue-specific and pathogen-response expression data. This approach enabled the identification of additional genes on that pathway, further demonstrating the utility of coexpression-based approaches. The network constructed as part of this work revealed relationships among the expression patterns of additional carrot FAD2s not functionally characterized here (for example, DCAR_017011, DCAR_003420, DCAR_002026, and DCAR_013553; Fig. 4; Supplemental Fig. S5). Based on their sequences, it is very difficult to predict the activity of the enzymes encoded by these genes (e.g. desaturation, acetylenation, hydroxylation). However, it seems possible that patterns in their expression are the basis for a particular aspect of polyacetylene biosynthesis in carrot, for example, polyacetylene biosynthesis in leaves or polyacetylene biosynthesis enhancement during stress. It will be interesting to see whether future studies will demonstrate

that coexpression analysis can provide more nuanced insights into such aspects of specialized metabolic pathways.

Based on structural comparisons between dehydrocrepenynate and the simplest falcarin-type polyacetylene (falcarinol), it seems likely that a Δ14 acetylenase, an ω-3 hydroxylase, as well as machinery that catalyze ω-desaturation and head group removal in carrot remain to be identified. These analyses indicated that there were 24 *FAD2* genes in the carrot genome and we explored the functions of six of these (Supplemental Fig. S7). The propensity of FAD2 enzymes to catalyze in-chain redox transformations on fatty acids not only suggests that one of these unexplored subsets of carrot *FAD2* genes might encode enzymes with Δ14 acetylenase and possibly ω-3 hydroxylase activity, but also that the catalysts for other remaining steps may reside outside the *FAD2* family. This raises questions about the reasons for such a high number of *FAD2* genes in carrot and whether they participate in specialized metabolic pathways besides linoleate and polyacetylene biosynthesis. From a chemical perspective, carrot root extracts have been studied in detail numerous times (for example, Zidorn et al., 2005; Schmiech et al., 2009), so it seems somewhat unlikely that unknown specialized compounds biosynthesized in part by FAD2 enzymes remain undiscovered. Though this possibility cannot be ruled out, a more likely explanation for the high number of carrot FAD2s is that some carrot FAD2s (1) mediate linole(n)ate biosynthesis with seed-enhanced expression, (2) participate in basal polyacetylene biosynthesis with periderm-enhanced expression, (3) participate in enhancing polyacetylene biosynthesis in response to pathogen attack, and (4) participate in some or all of these processes, such that there are multiple genes with redundant function.

Polyacetylene Structural Diversity

To lay further groundwork for future studies of the carrot polyacetylene pathway, we describe here a detailed analysis of the EI-MS fragmentation patterns of falcarin-type polyacetylenes. To enrich the EI-MS data, spectra were collected from each of the five detected polyacetylenes at not only the typical 70 eV ionization energy, but also at 10, 20, and 40 eV, then the spectra were merged to generate a composite mass spectrum for each compound. Other TMS-derivatized linear aliphatic compounds with secondary functional groups generate prominent α-fragments under electron ionization (see, for example, Schulz et al., 2000), with the corresponding peaks being among the most abundant in the resulting spectra. In contrast, the polyacetylenes falcarinol, falcarindiol, and falcarindiol-3-acetate, though they bear TMS-derivatized secondary functional groups, do not appear to generate strong α-fragments (Fig. 1). Unlike most other linear aliphatics, the secondary functional groups in these polyacetylenes are flanked on all sides by double or triple carbon-carbon bonds, hinting that these bonds may prohibit α-fragmentation. Such inhibition is consistent with the higher energy, less stable radicals that, if α-fragmentation were to take place, would form in the sp^2 or sp hybridized orbitals at the intersection of such functional groups.

Apart from falcarinol, falcarindiol, and falcarindiol-3-acetate, the TLC/GC-MS analyses performed here revealed two additional compounds. In contrast to the three polyacetylenes mentioned above, these two compounds did generate likely α-fragments, suggesting that their structures contained secondary functional groups with single carbon-carbon bonds on at least one side. The mass spectral signatures of these compounds and those of their hydrogenated and subsequently reduced derivatives pointed to their total carbon number as well as the position and oxidation state of the oxygen-containing functional groups in these compounds. Further guided by the comparisons of these spectra with the mass spectral signatures of falcarinol, falcarindiol, and falcarindiol-3-acetate, as well as the structures of previously identified carrot polyacetylenes (Schmiech et al., 2009), we tentatively identified these compounds as two novel carrot polyacetylenes, falcarintriol-8-acetate and falcarintriol-9-acetate.

The confirmed features of the new polyacetylenic compounds reported here, together with the structures of previously reported polyacetylenes from the Asterids (for review, see Minto and Blacklock, 2008; Dawid et al., 2015; Negri, 2015) point to substantial structural diversity among falcarin-type polyacetylenic metabolites. This diversity includes structures with one to three or more oxygen-containing functional groups on several positions of the aliphatic chain that can occupy various oxidation states, as well as multiple possible hydroxyl group decorations such as acetylation and methylation. Thus, additional portions of falcarin-type polyacetylene biosynthesis appear to be composed of substantial installation and modification of functional groups around a common backbone. Such modifications and structural diversity are signatures of specialized metabolic pathways, and it will be interesting to see how these more complex compounds functionally contribute to the cocktail of polyacetylenes found in carrots.

MATERIALS AND METHODS

Plant Material, Growth Conditions, and Harvesting

Daucus carota subsp. *sativus* var Danvers seeds (USDA GRIN Global) were sown in plastic pots and grown in greenhouse conditions. Plants were harvested when roots reached a diameter of approximately 3 cm and were washed thoroughly under tap water. Leaf and petiole samples were harvested with scissors. Roots were carefully dissected into 2.5-cm-thick discs from which periderm, phloem, and xylem samples were isolated using a clean razor. Whole-root tissue samples were prepared by grating into thin strips. All samples were immediately frozen in liquid N_2 and lyophilized.

TLC Separation of Polyacetylenes and Chemical Structure Analyses

Lyophilized whole root samples (approximately 200 mg) were ground in a coffee mill, transferred to a glass extraction tube, suspended in ethyl acetate (Sigma; 4 mL), and mechanically homogenized (OMNI THQ, 16,000 rpm, 2 min). The homogenate was centrifuged (Eppendorf 5702, 4 min, 3,000*g*), the resulting supernatant was transferred to a new glass tube, washed with sodium chloride (50% v/v [saturated sodium chloride] 2 mL), then the supernatant was again transferred to a new glass tube, evaporated under N_2 at 70°C, the residue was dissolved in ethyl acetate (500 µL), and finally it was loaded onto a TLC plate (EMD, 20 × 20 cm, 200 µm thickness) with a capillary tube. The plate was developed in 3:1 heptane:ethyl acetate, resulting bands were visualized by primuline staining (Sigma; 1% v/v [acetone saturated with primuline] in acetone), scraped, then extracted with ethyl acetate. An aliquot of each extract was transferred to a GC vial (Agilent), and the solvent was evaporated under N_2 at 70°C. The residue was then derivatized by dissolving it in dry pyridine (Sigma; 25 µL), adding *N*,*O*-bis(TMS)trifluoroacetamide (Sigma; 25 µl), and allowing the mixture to incubate (70°C, 45 min). Finally, the excess derivatization reagents were evaporated under N_2 at 70°C and the residue was dissolved in ethyl acetate (50 µL).

Once prepared, samples were immediately analyzed with a GC-MS system (Agilent 7890A GC) equipped with a split-splitless injector (carrier gas, H_2; injection temperature, 300°C; inlet pressure, 7.9 psi; total flow, 6.5 mL/min; septum purge flow, 2 mL/min; split ratio, 5:1; split flow, 3.75 mL/min; column flow, 0.75 mL/min), a HP-1 capillary column (Agilent, 30m, 0.25 mm inner diameter, 0.25 µm film thickness), and a temperature-programmable oven (initial temperature, 175°C; ramp, 10°C/min to 260°C; then hold for 8 min), and a mass spectral detector (Agilent 5975C EI/CI MS; *m/z* 40–600, 1 scan/s).

Hydrogenation reactions were carried out by adding the following to a GC vial: heptane (200 µL), a small aliquot of a TLC fraction, and a catalytic amount of palladium on carbon (Sigma), followed by purging with H_2 gas and shaking vigorously (30 min). After this, the vial was centrifuged (4 min, 3000*g*), the supernatant was transferred to a new GC vial, the solvent was evaporated, and the residue was derivatized and analyzed with GC-MS as described above. Reduction reactions were carried out by adding to a GC vial the following: dry diethyl ether (200 µL), a small aliquot of a TLC fraction, and lithium aluminum hydride powder (Sigma; approximately 2 mg), then allowing the mixture to incubate (room temp., 30 min) with occasional vortex mixing. After incubation, the reaction was quenched by the slow addition of ethyl acetate (200 µL), partitioned against water (100 µL), then the supernatant was transferred to a new GC vial, derivatized, and analyzed with GC-MS, as described above.

Standards for oleate, linoleate, crepenynate, and dehydrocrepenynate were acquired by transmethylating *fad3fae1 Camelina sativa* seeds (high oleic), *Crepis alpina* seeds (high crepenynic), and *Cantharellus* fruiting bodies (chanterelle; high dehydrocrepenynic), respectively (2.5% v/v H_2SO_4 in methanol, 2 mL, 90°C, 45 min). Hexane extracts from the transmethylation reactions were purified via TLC and analyzed with GC-MS as described previously (Cahoon et al., 2003); the spectra from these standards were consistent with spectra of the same compounds as published.

Quantitative Analysis of Polyacetylenes by Gas Chromatography

Aliquots of dry tissue were weighed and placed in individual glass lipid extraction tubes, suspended in ethyl acetate (300 µL), spiked with linolenyl alcohol internal standard (Nu-Check Prep, 5 µg), and mechanically homogenized (OMNI THQ, 16k rpm, 30 s) on ice. Sodium chloride (50% v/v [saturated sodium chloride], 100 µL) was added to the homogenate, which was vortexed (10 s), then centrifuged (4 min, 3000*g*). An aliquot of the supernatant (200 µL) was transferred to a GC vial with an insert (Agilent), the solvent was evaporated at 70°C under nitrogen gas, and the residue was derivatized and analyzed with GC-MS as described above. Samples were analyzed immediately after preparation.

To correct for differences in ionization efficiency between each analyte and the internal standard, the TLC samples described above were spiked with linolenyl internal standard, derivatized, and analyzed with both the GC-MS system described above and a gas chromatography system equipped with a flame ionization detector (Agilent, 275°C, 45 mL/min H_2, 375 mL/min air; INNOWAX column, 30 m, 0.25 mm inner diameter, 0.25 µm film thickness). Though it does not provide structural information, gas chromatography-flame ionization detection provides quantitative information that is not biased by ionization efficiency. The ratio of analyte:standard, as detected by the mass spectral detector versus the flame ionization detector, was used to normalize the results from the GC-MS system and provide quantitative measures of polyacetylenes from each carrot tissue sample.

Analysis of Carrot FAD2 Amino Acid and Nucleotide Sequences

The amino acid sequences of the carrot FAD2s were aligned with the amino acid sequences of previously characterized FAD2-like enzymes (for accession numbers, see Supplemental Table S3) from other plant species using the MUSCLE algorithm (Edgar, 2004), implemented using the 'msa' package (Bodenhofer et al., 2015) in R (R Core Development Team, 2015). The level of consensus at each position in the alignment and its correlation with FAD2 desaturase or diverged FAD2-like activity was calculated using a custom R script. The coding sequences of the carrot FAD2s were codon-aligned using the 'orthologr' package (Drost et al., 2015). Phylogenetic trees were reconstructed from peptide alignments that were aligned onto the coding sequences with PAL2NAL v13 (Suyama et al., 2006). Alignments were filtered using two criteria via TRIMAL (Capella-Gutiérrez et al., 2009). The alignments were removed if gaps were observed in more than 90% of sequences or covered less than 30% of the total alignment length for the sequences. Maximum likelihood gene trees were estimated using RAxML v7.3.0 (Stamatakis, 2006) with the general time reversible + Γ substitution model and 1,000 bootstrap replicates. The tree was rooted to a *Physcomitrella patens* FAD2. Reconstructed phylogenetic trees were visualized and annotated in R with the package 'ggtree' (Yu et al., 2017).

Culturing of and Treatment of Carrot Root Discs with *Sclerotinia sclerotiorum*

From long-term storage, sclerotia of *Sclerotinia sclerotiorum* isolate Scl02-05 were transferred to potato dextrose agar (BD Company) plates and incubated in the dark at room temperature. Agar plugs were taken from the leading edge of the expanding colony with a dental filling carrier 2-mm-end instrument and applied on the taproot disks of Danvers Half Long carrots. *S. sclerotiorum* inoculated root disks were incubated in the dark, in petri dishes containing humid paper towels to mimic optimal conditions for fungal infections. For GC-MS and FID-MS analyses, control disks were harvested immediately, and inoculated disks were harvested 24 h postinoculations.

Culturing and Elicitation of Carrot Cell Suspensions, RNA Extraction, Preparation of RNA-Seq Libraries, and Sequencing

Carrot seeds were germinated on sterile Murashige and Skoog plates, and 2-week-old seedlings were dissected with a sterile scalpel and transferred to callus-inducing plates (solid callus medium; Supplemental Table S1). After 2 weeks, calli were transferred to callus medium and allowed to grow for 2 weeks. Finally, calli were transferred to a liquid culture medium (liquid callus medium; Supplemental Table S1) and placed on a shaker (120 rpm) under ambient light and subcultured every 2 weeks.

A fungal elicitor was prepared from *Phytopthora megasperm* cell walls as previously described (Ayers et al., 1976). In brief, mycelia of *Phytophthora megasperma* f.sp. *glycinea* were washed with water, homogenized, then washed sequentially with Tris/EDTA, water, chloroform/methanol, and acetone, then allowed to dry. The cell wall residue (4 g) was suspended in water (200 mL), autoclaved for 3 h, filtered, dried using a rotary evaporator, resuspended in water (2 mL), dialyzed against water (8 L, 24 h), filtered (0.45-mm membrane filter), lyophilized, and resuspended in water (1,000 µL). This elicitor preparation was used to elicit carrot cell suspensions (200 µL elicitor per 200 mL cell suspension). RNA was extracted from carrot cell suspensions both before and 8 h after elicitation (two replicates for each time point) using the TRIzol method according to the manufacturer's instructions (Invitrogen). cDNA libraries were constructed and sequenced as described previously (Troncoso-Ponce et al., 2011).

Transcript Abundance Estimation and Coexpression Analysis

The raw reads from this study and the SRA public database (20 samples) were filtered using Trimmomatic (trim leading parameter 3 bp, trim trailing

parameter 3 bp, sliding window parameters 4 bp less than quality score 15, and minimum length with 36 bp LEADING:3 TRAILING:3 SLIDINGWINDOW:4:15 MINLEN:36; Bolger et al., 2014). Filtered reads were aligned to the *D. carota* genome v.2.0 (Iorizzo et al., 2016) using HISAT2 (Kim et al., 2015a) with minimum intron length 20 bp and maximum intron length 6,000 bp (–min-intronlen 20 and –max-intronlen 6,000). The mapped reads were converted and sorted by Samtools (Li et al., 2009). The raw read count matrix was obtained using featureCount in R via the Rsubread package (Liao et al., 2013) with the *D. carota* v.2.0 GTF annotation file. The TPM values were determined with raw count reads following numbers of reads assigned to gene features. Differential expression analysis was quantified using the DESeq2 package (Love et al., 2014). PCC were measured in a pairwise analysis across the TPM value in the *D. carota* genome by FastGCN (Liang et al., 2015). The criteria of PCC networks were FDR-adjusted P value ($q < 0.1$) and Z-score ($z \geq 3.29$).

RT-qPCR

Total RNA was isolated from periderm, phloem, and xylem of full-grown taproots (10-12 weeks old) of Danvers Half Long carrots. RNA extraction was performed using the Direct-zol RNA Mini-prep (Zymo Research) kit according to the manufacturer's instructions. For cDNA synthesis, iScript Reverse Transcription Supermix (BioRad) was used. The RT-qPCR were carried out using the Apex qPCR GREEN Master Mix (Apex Bioresearch Products) according to the manufacturer's instructions. The RT-qPCR reactions were performed on a CFX96 Touch Real-Time PCR Detection System (BioRad), with four biological replicates, each with two technical replicates. Transcripts were quantified using the relative CT (ΔCT) method and normalized using the endogenous control gene DcActin (Tian et al., 2015). The primers used for RT-qPCR are listed in Supplemental Table S1.

Gene Cloning, Vector Construction, Heterologous Expression, and Fatty Acid Analysis

Genomic DNA was extracted from carrot leaf tissue using the DNEasy Plant Mini Kit according to the manufacturer's protocol (Qiagen). Since carrot FAD2s do not contain predicted introns, they were cloned directly from genomic DNA by PCR using gene-specific primers (see Supplemental Table S2).

To screen for oleate Δ12 desaturase activity, carrot FAD2s were expressed in yeast (*Saccharomyces cerevisiae*) strain BY4147. For this, fragments from cloning PCRs (see above) were used as templates for a second round of PCR to amplify the coding sequence of each FAD2-like gene, add a 15-base pair adapter to either end, and add the yeast consensus sequence (A/Y)A(A/C)A(A/C)A immediately upstream of the start codon. The adapters were complementary to the regions before and after the *Bam*HI and *Eco*RI sites, respectively, in the pYES vector (details about adding the yeast transcription sequence). These PCR products were ligated into the *Bam*HI/*Eco*RI double-digested pYES vector using the In-Fusion HD Cloning Kit (Takara Bio) according to the manufacturer's instructions. The sequences of the resulting vectors were verified using PCR, restriction digestion, and Sanger sequencing.

pYES vectors harboring carrot genes were transformed into *Saccharomyces cerevisiae* strain BY4147 using the Frozen-EZ Yeast Transformation II Kit (Zymogen) according to the manufacturer's instructions. Transformants, grown at 28°C, were selected on plates lacking uracil (YPD Media A; Supplemental Table S1), then transferred to liquid media (liquid YPD Media C, noninductive; Supplemental Table S1), and grown at 28°C for 4 d. To induce expression of the transgene, yeast cultures were washed with water (3×), resuspended in induction medium (liquid YPD Media C, inductive; Supplemental Table S1), and grown for 7 d at 28°C.

To screen for linoleate Δ12 acetylenase activity or crepenynate Δ14 desaturase activity, carrot FAD2s were expressed in Arabidopsis (*Arabidopsis thaliana*) seeds. For this, fragments from the initial cloning PCR (see above) were used as templates for PCR reactions to amplify the coding sequence of each FAD2 and add 15 base pair adapters to either end. These adapters were complementary to the regions before and after the *Eco*RI and *Xba*I sites, respectively, in the pBINGlyRed3 vector (Kim et al., 2015b). These PCR products were ligated into the double-digested vector using the In-Fusion HD Cloning Kit (Takara Bio) according to the manufacturer's instructions and verified as described above for the pYES vectors.

pBINGlyRed3 vectors harboring carrot genes were transformed into *Agrobacterium* (*Agrobacterium tumefaciens*) GV3101::pMP90 by electroporation. Transformed bacteria were cultured at 28°C, pelleted, then suspended in 1/2 Murashige and Skoog with Suc (30 g), at pH 5.8. Developing flowers of greenhouse-grown Arabidopsis *fad3fae1* mutant plants (Smith et al., 2003) were dipped into the suspended agrobacteria, kept in the dark overnight, returned to the greenhouse until seeds fully developed, followed by selection for transformants using red fluorescence imparted by the DsRed gene contained in the pBINGlyRed3 vector. Since the intent was not to assess enzyme activity level or stability or physiology of transgenic Arabidopsis lines, but rather to simply test for specific enzyme activities, 10 independent transgenic Arabidopsis seeds harboring identical constructs were pooled and screened at the T1 stage as described for previous screens of acyl-ACP desaturase activity (Cahoon and Shanklin, 2000).

Fatty acid profiles of both yeast and transgenic Arabidopsis seeds were measured with GC by heptane extraction of transmethylation products.

Accession Numbers

Sequence data used in this work can be found in the Phytozome/GenBank databases under the accession numbers listed in Supplemental Table S3.

Supplemental Data

The following supplemental materials are available.

Supplemental Figure S1. Mass spectra of synthetic polyacetylene standards and compounds 1.1 and 3.1 extracted from carrot.

Supplemental Figure S2. Location of *FAD2* genes in carrot chromosomes.

Supplemental Figure S3. Complete multiple sequence alignment of previously characterized plant FAD2 proteins and FAD2 proteins predicted from the carrot genome.

Supplemental Figure S4. Polyacetylene abundance in carrots before and after treatment with *Sclerotinia sclerotiorum*.

Supplemental Figure S5. Expression of carrot *FAD2* genes in diverse carrot tissues and carrot cell suspensions.

Supplemental Figure S6. Transcript abundances of canonical and divergent *FAD2* genes in carrot periderm, phloem, and xylem as measured by qRT-PCR.

Supplemental Figure S7. Functional characterization of FAD2s from carrot.

Supplemental Figure S8. Functional characterization of FAD2s from carrot.

Supplemental Figure S9. Syntenic relationships supporting the emergence of *FAD2* and divergent *FAD2* relationships among carrot, lettuce, and sunflower.

Supplemental Figure S10. model crystal structure of the *Petroselinum crispum* FAD2.

Supplemental Table S1. Media used in this work.

Supplemental Table S2. List of primers used in this work.

Supplemental Table S3. Accession numbers of genes analyzed as part of this work.

ACKNOWLEDGMENTS

We wish to acknowledge Lu Gan for advice on gene cloning and vector construction, Evan Updike for assistance with transforming Arabidopsis plants and selecting transgenic seeds, Samantha Link for careful monitoring of carrot plants, Zach Wahrenburg for helpful discussions of polyacetylene purification, Reinhard Jetter for providing comments on an early version of the manuscript, Brett Tylerfor providing the *Phytopthora* cell walls, and the RTSF Genomics Core at Michigan State University for sequencing services.

Received September 26, 2018; accepted October 11, 2018; published October 17, 2018.

LITERATURE CITED

Adlof RO, Emken EA (1993) Large-scale preparation of linoleic acid-d2-enriched triglycerides from *Crepis alpina* seed oil. J Am Oil Chem Soc **70**: 817–819

Ayers AR, Ebel J, Valent B, Albersheim P (1976) Host-pathogen interactions. X. Fractionation and biological activity of an elicitor isolated from the mycelial walls of *Phytophthora megasperma* var. sojae. Plant Physiol **57**: 760–765

Badami RC, Patil KB (1980) Structure and occurrence of unusual fatty acids in minor seed oils. Prog Lipid Res **19**: 119–153

Barley GC, Jones ERH, Thaller V (1988) Crepenynate as a precursor of falcarinol in carrot tissue culture. *In* **J Lam, H Breteler, T Arnason, L Hansen**, eds, Chemistry and Biology of Naturally-Occurring Acetylenes and Related Compounds, Vol. 7. Elsevier Science, New York, pp 85–91

Bernart MW, Cardellina II JH, Balaschak MS, Alexander MR, Shoemaker RH, Boyd MR (1996) Cytotoxic falcarinol oxylipins from *Dendropanax arboreus*. J Nat Prod **59**: 748–753

Blacklock BJ, Scheffler BE, Shepard MR, Jayasuriya N, Minto RE (2010) Functional diversity in fungal fatty acid synthesis: the first acetylenase from the Pacific golden chanterelle, *Cantharellus formosus*. J Biol Chem **285**: 28442–28449

Bodenhofer U, Bonatesta E, Horejš-Kainrath C, Hochreiter S (2015) msa: an R package for multiple sequence alignment. Bioinformatics **31**: 3997–3999

Bohlman F (1988) Naturally-occurring acetylenes. *In* **J Lam, H Breteler, T Arnason, L Hansen**, eds, Chemistry and Biology of Naturally-Occurring Acetylenes and Related Compounds, Vol. 7. Elsevier Science, New York, pp 1–19

Bolger AM, Lohse M, Usadel B (2014) Trimmomatic: a flexible trimmer for Illumina sequence data. Bioinformatics **30**: 2114–2120

Broadwater JA, Whittle E, Shanklin J (2002) Desaturation and hydroxylation. Residues 148 and 324 of Arabidopsis FAD2, in addition to substrate chain length, exert a major influence in partitioning of catalytic specificity. J Biol Chem **277**: 15613–15620

Broun P, Shanklin J, Whittle E, Somerville C (1998) Catalytic plasticity of fatty acid modification enzymes underlying chemical diversity of plant lipids. Science **282**: 1315–1317

Cahoon EB, Kinney AJ (2005) The production of vegetable oils with novel properties: using genomic tools to probe and manipulate plant fatty acid metabolism. Eur J Lipid Sci Technol **107**: 239–243

Cahoon EB, Shanklin J (2000) Substrate-dependent mutant complementation to select fatty acid desaturase variants for metabolic engineering of plant seed oils. Proc Natl Acad Sci USA **97**: 12350–12355

Cahoon EB, Carlson TJ, Ripp KG, Schweiger BJ, Cook GA, Hall SE, Kinney AJ (1999) Biosynthetic origin of conjugated double bonds: production of fatty acid components of high-value drying oils in transgenic soybean embryos. Proc Natl Acad Sci USA **96**: 12935–12940

Cahoon EB, Schnurr JA, Huffman EA, Minto RE (2003) Fungal responsive fatty acid acetylenases occur widely in evolutionarily distant plant families. Plant J **34**: 671–683

Capella-Gutiérrez S, Silla-Martínez JM, Gabaldón T (2009) trimAl: a tool for automated alignment trimming in large-scale phylogenetic analyses. Bioinformatics **25**: 1972–1973

Cunsolo F, Ruberto G, Amico V, Piattelli M (1993) Bioactive metabolites from Sicilian marine fennel, *Crithmum maritimum*. J Nat Prod **56**: 1598–1600

Czepa A, Hofmann T (2003) Structural and sensory characterization of compounds contributing to the bitter off-taste of carrots (*Daucus carota* L.) and carrot puree. J Agric Food Chem **51**: 3865–3873

Dawid C, Dunemann F, Schwab W, Nothnagel T, Hofmann T (2015) Bioactive C_{17}-polyacetylenes in carrots (*Daucus carota* L.): current knowledge and future perspectives. J Agric Food Chem **63**: 9211–9222

De Wit PJGM, Kodde E (1981) Induction of polyacetylenic phytoalexins in Lycopersicon esculentum after inoculation with *Cladosporium fulvum* (syn. *Fulvia fulva*). Physiol Plant Pathol **18**: 143–148

Drost HG, Gabel A, Grosse I, Quint M (2015) Evidence for active maintenance of phylotranscriptomic hourglass patterns in animal and plant embryogenesis. Mol Biol Evol **32**: 1221–1231

Edgar RC (2004) MUSCLE: multiple sequence alignment with high accuracy and high throughput. Nucleic Acids Res **32**: 1792–1797

Elgahme NFA, Wittstock U (2018) Quantitative profiling of polyacetylenes in tissue cultures and plant parts of three species of the Asteraceae. Plant Cell Tissue Organ Cult **134**: 251–265

Elgersma DM, Liem JI (1989) Accumulation of phytoalexins in susceptible and resistant near-isogenic lines of tomato infected with *Verticillium albo-atrum* or *Fusarium oxysporum* f.sp. *lycopersici*. Physiol Mol Plant Pathol **34**: 545–555

Fujimoto Y, Satoh M (1988) A new cytotoxic chlorine-containing polyacetylene from the callus of Panax ginseng. Chem Pharm Bull (Tokyo) **36**: 4206–4208

Garrod B, Lewis BG, Coxon DT (1978) Cis-heptadeca-1,9-diene-4,6-diyne-3,8-diol, an antifungal polyacetylene from carrot root tissue. Physiol Plant Pathol **13**: 241–246

Haigh WG, Morris LJ, James AT (1968) Acetylenic acid biosynthesis in *Crepis rubra*. Lipids **3**: 307–312

Harding VK, Heale JB (1980) Isolation and identification of the antifungal compounds accumulating in the induced resistance response of carrot root slices to *Botrytis cinerea*. Physiol Plant Pathol **17**: 277–289

Harding VK, Heale JB (1981) The accumulation of inhibitory compounds in the induced resistance response of carrot root slices to *Botrytis cinerea*. Physiol Plant Pathol **18**: 7–15

Haritos VS, Horne I, Damcevski K, Glover K, Gibb N, Okada S, Hamberg M (2012) The convergent evolution of defensive polyacetylenic fatty acid biosynthesis genes in soldier beetles. Nat Commun **3**: 1150

Hornung E, Pernstich C, Feussner I (2002) Formation of conjugated Δ11Δ13-double bonds by Δ12-linoleic acid (1,4)-acyl-lipid-desaturase in pomegranate seeds. Eur J Biochem **269**: 4852–4859

Iorizzo M, Ellison S, Senalik D, Zeng P, Satapoomin P, Huang J, Bowman M, Iovene M, Sanseverino W, Cavagnaro P, (2016) A high-quality carrot genome assembly provides new insights into carotenoid accumulation and asterid genome evolution. Nat Genet **48**: 657–666

Jones ERH, Safe S, Thaller V (1966) Natural acetylenes. Part XXIII. A C_{18} polyacetylenic keto-aldehyde related to falcarinone from an umbellifer (*Pastinaca sativa* L.). J Chem Soc C **1966**: 1220–1221

Kawazu K, Noguchi H, Fujishita K, Iwasa J, Egawa H (1973) Two new antifungal compounds from *Dendropanax trifidus*. Tetrahedron Lett **14**: 3131–3132

Kemp MS (1978) Falcarindiol: an antifungal polyacetylene from *Aegopodium podagraria*. Phytochemistry **17**: 1002

Kim D, Langmead B, Salzberg SL (2015a) HISAT: a fast spliced aligner with low memory requirements. Nat Methods **12**: 357–360

Kim HJ, Silva JE, Vu HS, Mockaitis K, Nam JW, Cahoon EB (2015b) Toward production of jet fuel functionality in oilseeds: identification of FatB acyl-acyl carrier protein thioesterases and evaluation of combinatorial expression strategies in Camelina seeds. J Exp Bot **66**: 4251–4265

Kirsch C, Hahlbrock K, Somssich IE (1997) Rapid and transient induction of a parsley microsomal delta 12 fatty acid desaturase mRNA by fungal elicitor. Plant Physiol **115**: 283–289

Kobaek-Larsen M, Christensen LP, Vach W, Ritskes-Hoitinga J, Brandt K (2005) Inhibitory effects of feeding with carrots or (-)-falcarinol on development of azoxymethane-induced preneoplastic lesions in the rat colon. J Agric Food Chem **53**: 1823–1827

Kosma DK, Rice A, Pollard M (2015) Analysis of aliphatic waxes associated with root periderm or exodermis from eleven plant species. Phytochemistry **117**: 351–362

Li H, Handsaker B, Wysoker A, Fennell T, Ruan J, Homer N, Marth G, Abecasis G, Durbin R. (2009) The sequence alignment/map format and SAMtools. Bioinformatics **25**: 2078–2079.

Liang M, Zhang F, Jin G, Zhu J (2015) FastGCN: a GPU accelerated tool for fast gene co-expression networks. PLoS One **10**: e0116776

Liao Y, Smyth GK, Shi W (2013) The Subread aligner: fast, accurate and scalable read mapping by seed-and-vote. Nucleic Acids Res **41**: e108

Love MI, Huber W, Anders S (2014) Moderated estimation of fold change and dispersion for RNA-seq data with DESeq2. Genome Biol **15**: 550

Matsunaga H, Katano M, Yamamoto H, Mori M, Takata K (1989) Studies on the panaxytriol of Panax ginseng C. A. Meyer. Isolation, determination and antitumor activity. Chem Pharm Bull (Tokyo) **37**: 1279–1281

Matsunaga H, Katano M, Yamamoto H, Fujito H, Mori M, Takata K (1990) Cytotoxic activity of polyacetylene compounds in Panax ginseng C. A. Meyer. Chem Pharm Bull (Tokyo) **38**: 3480–3482

Minto RE, Blacklock BJ (2008) Biosynthesis and function of polyacetylenes and allied natural products. Prog Lipid Res **47**: 233–306

Nam JW, Kappock TJ (2007) Cloning and transcriptional analysis of *Crepis alpina* fatty acid desaturases affecting the biosynthesis of crepenynic acid. J Exp Bot **58**: 1421–1432

Negri R (2015) Polyacetylenes from terrestrial plants and fungi: recent phytochemical and biological advances. Fitoterapia **106**: 92–109

Olsson K, Svensson R (1996) The influence of polyacetylenes on the susceptibility of carrots to storage diseases. J Phytopathol (1986) **144**: 441–447

Pochapsky TC, Kazanis S, Dang M (2010) Conformational plasticity and structure/function relationships in cytochromes P450. Antioxid Redox Signal **13**: 1273–1296

R Core Development Team (2015) R: a language and environment for statistical computing. The R Foundation for Statistical Computing. http://www.r-project.org

Roman M, Dobrowolski JC, Baranska M, Baranski R (2011) Spectroscopic studies on bioactive polyacetylenes and other plant components in wild carrot root. J Nat Prod (Gorakhpur) **74**: 1757–1763

Rubatzky VE, Quiros CF, Simon PW (1999) Carrots and Related Vegetable Umbelliferae. CABI, New York

Schmiech L, Alayrac C, Witulski B, Hofmann T (2009) Structure determination of bisacetylenic oxylipins in carrots (*Daucus carota* L.) and enantioselective synthesis of falcarindiol. J Agric Food Chem **57**: 11030–11040

Schulz S, Arsene C, Tauber M, McNeil JN (2000) Composition of lipids from sunflower pollen (*Helianthus annuus*). Phytochemistry **54**: 325–336

Shanklin J, Whittle E, Fox BG (1994) Eight histidine residues are catalytically essential in a membrane-associated iron enzyme, stearoyl-CoA desaturase, and are conserved in alkane hydroxylase and xylene monooxygenase. Biochemistry **33**: 12787–12794

Smith MA, Moon H, Chowrira G, Kunst L (2003) Heterologous expression of a fatty acid hydroxylase gene in developing seeds of *Arabidopsis thaliana*. Planta **217**: 507–516

Somssich IE, Bollmann J, Hahlbrock K, Kombrink E, Schulz W (1989) Differential early activation of defense-related genes in elicitor-treated parsley cells. Plant Mol Biol **12**: 227–234

Sperling P, Lee M, Girke T, Za U, Stymne S, Heinz E (2000) A bifunctional Δ6-fatty acyl acetylenase / desaturase from the moss *Ceratodon purpureus*. A new member of the cytochrome b5 superfamily. Eur J Biochem **267**: 3801–3811

Stamatakis A (2006) RAxML-VI-HPC: maximum likelihood-based phylogenetic analyses with thousands of taxa and mixed models. Bioinformatics **22**: 2688–2690

Suyama M, Torrents D, Bork P (2006) PAL2NAL: robust conversion of protein sequence alignments into the corresponding codon alignments. Nucleic Acids Res **34**: W609–W612

Tian C, Jiang Q, Wang F, Wang GL, Xu ZS, Xiong AS (2015) Selection of suitable reference genes for qPCR normalization under abiotic stresses and hormone stimuli in carrot leaves. PLoS One **10**: e0117569

Troncoso-Ponce MA, Kilaru A, Cao X, Durrett TP, Fan J, Jensen JK, Thrower NA, Pauly M, Wilkerson C, Ohlrogge JB (2011) Comparative deep transcriptional profiling of four developing oilseeds. Plant J **68**: 1014–1027

Wang H, Klein MG, Zou H, Lane W, Snell G, Levin I, Li K, Sang B-C (2015) Crystal structure of human stearoyl-coenzyme A desaturase in complex with substrate. Nat Struct Mol Biol **22**: 581–585

Wisecaver JH, Borowsky AT, Tzin V, Jander G, Kliebenstein DJ, Rokas A. (2017) A global co-expression network approach for connecting genes to specialized metabolic pathways in plants. Plant Cell **29**: 944–959.

Yu G, Smith DK, Zhu H, Guan Y, Lam TTY (2017) Ggtree: an R package for visualization and annotation of phylogenetic trees with their covariates and other associated data. Methods Ecol Evol **8**: 28–36

Zidorn C, Jöhrer K, Ganzera M, Schubert B, Sigmund EM, Mader J, Greil R, Ellmerer EP, Stuppner H (2005) Polyacetylenes from the Apiaceae vegetables carrot, celery, fennel, parsley, and parsnip and their cytotoxic activities. J Agric Food Chem **53**: 2518–2523